THE JOURNAL OF BIOLOGICAL CHEMISTRY VOL. 280, NO. 49, pp. 40668–40675, December 9, 2005

Structural Studies on a Mitochondrial Glyoxalase II*

Received for publication, September 6, 2005, and in revised form, October 3, 2005 Published, JBC Papers in Press, October 14, 2005, DOI 10.1074/jbc.M509748200

Gishanthi P. K. Marasinghe[‡], Ian M. Sander[‡], Brian Bennett[§], Gopalraj Periyannan[‡], Ke-Wu Yang[‡], Christopher A. Makaroff[‡], and Michael W. Crowder[‡1]

From the [‡]Department of Chemistry and Biochemistry, Miami University, Oxford, Ohio 45056 and the [§]National Biomedical EPR Center, Department of Biophysics, Medical College of Wisconsin, Milwaukee, Wisconsin 53226-0509

Glyoxalase 2 is a β-lactamase fold-containing enzyme that appears to be involved with cellular chemical detoxification. Although the cytoplasmic isozyme has been characterized from several organisms, essentially nothing is known about the mitochondrial proteins. As a first step in understanding the structure and function of mitochondrial glyoxalase 2 enzymes, a mitochondrial isozyme (GLX2-5) from *Arabidopsis thaliana* was cloned, overexpressed, purified, and characterized using metal analyses, EPR and ^{1}H NMR spectroscopies, and x-ray crystallography. The recombinant enzyme was shown to bind 1.04 ± 0.15 eq of iron and 1.31 ± 0.05 eq of Zn(II) and to exhibit k_{cat} and K_m values of 129 ± 10 s^{-1} and 391 ± 48 μM, respectively, when using *S*-D-lactoylglutathione as the substrate. EPR spectra revealed that recombinant GLX2-5 contains multiple metal centers, including a predominant Fe(III)Zn(II) center and an anti-ferromagnetically coupled Fe(III)Fe(II) center. Unlike cytosolic glyoxalase 2 from *A. thaliana*, GLX2-5 does not appear to specifically bind manganese. ^{1}H NMR spectra revealed the presence of at least eight paramagnetically shifted resonances that arise from protons in close proximity to a Fe(III)Fe(II) center. Five of these resonances arose from solvent-exchangeable protons, and four of these have been assigned to NH protons on metal-bound histidines. A 1.74-Å resolution crystal structure of the enzyme revealed that although GLX2-5 shares a number of structural features with human GLX2, several important differences exist. These data demonstrate that mitochondrial glyoxalase 2 can accommodate a number of different metal centers and that the predominant metal center is Fe(III)Zn(II).

The glyoxalase system consists of two enzymes, lactoylglutathione lyase (glyoxalase I, GLX1)[2] and hydroxyacylglutathione hydrolase (glyoxalase II, GLX2), that act coordinately to convert a variety of α-ketoaldehydes into hydroxy acids in the presence of glutathione (1). Aromatic and aliphatic α-ketoaldehydes react spontaneously with glutathione to form thiohemiacetals, which are converted to *S*-(2-hydroxyacyl)glutathione derivatives by GLX1. GLX2 hydrolyzes *S*-(2-hydroxyacyl)glutathione derivatives to regenerate glutathione and produce hydroxy acids. Glyoxalase I, a Zn(II) or Ni(II) metalloprotein, can utilize a number of α-ketoaldehydes (2). However, the primary physiological substrate of the enzyme is thought to be methylglyoxal (MG), a cytotoxic and mutagenic compound that is formed primarily as a by-product of carbohydrate and lipid metabolism (3, 4). MG can react with DNA to form modified guanylate residues (5) and interstrand cross-links (6). It also reacts with proteins to form glycosylamine derivatives of arginine and lysine and hemithioacetals with cysteines (7).

Cells with high glycolytic rates exhibit high rates of methylglyoxal formation and increased levels of GLX1 activity. For instance, increased levels of GLX1 and GLX2 RNA and protein have been detected in tumor cells, including breast carcinoma cells (8). Because selective inhibition of the glyoxalase system could cause cellular toxicity, the glyoxalase enzymes have been investigated as potential anti-tumor and anti-malarial targets in animal systems (1, 9). Inhibitors of GLX1 and GLX2 can inhibit the growth of tumor cells *in vitro* (10, 11) and *in vivo* (12) and have been shown to have anti-proliferative effects on parasitic infections (13). Finally, increased MG levels have been implicated with several complications associated with diabetes mellitus (1, 14, 15), and changes in glyoxalase enzymes have been linked with neurodegenerative disease (16). Therefore, high levels of MG and the glyoxalase enzymes are associated with several aspects of human disease.

GLXI has been studied extensively in a number of systems with biochemical, computational, and x-ray crystallographic studies providing considerable insight into its kinetic mechanism (reviewed in Refs. 17 and 18). Insight into the kinetic mechanism of GLX1 has allowed the development of new classes of mechanism-based, competitive inhibitors that can inhibit tumor growth *in vitro* and *in vivo* (12, 19, 20).

Considerably less is known about the structure, reaction mechanism, and physiological role(s) of GLX2. In contrast to GLX1, which is found as a single isozyme, GLX2 exists as multiple isozymes in many organisms, including yeast, plants, and animals. GLX2 activity has been found in both the cytosol and mitochondria (21–23). Furthermore, GLX2 isozymes were found in both the matrix and inter-membrane space of rat liver mitochondria (24, 25). In most cases, separate genes encode the cytosolic and mitochondrial isozymes. However, in humans a single gene produces both cytosolic and mitochondrial GLX2 (21). Therefore, the physiological role(s) of GLX2 may be more complex than GLX1.

S-D-Lactoylglutathione (SLG) appears to be the preferred substrate for GLX2 from most sources, including human, yeast, and plants (26–33). However, GLX2 can hydrolyze many different glutathione thioesters, including *S*-D-mandeloylglutathione, *S*-D-acetylglutathione, *S*-D-acetoacetylglutathione, *S*-D-formylglutathione, *S*-D-glycolylglutathione, and *S*-D-lactonylglutathione. Most interestingly, glyoxalase II isolated from African trypanosomes prefers thioesters of trypanothione as substrates (34).

GLX2 is one of many protein families characterized to date that contain a metallo-β-lactamase fold. The metallo-β-lactamases typically bind Zn(II) (35, 36), whereas the rubredoxin:oxygen oxidoreductase and ZiPD families contain di-Fe and di-Zn centers, respectively (37, 38). *Arabidopsis* cytoplasmic GLX2 (GLX2-2) can bind Zn(II), Fe, and Mn (39–41), whereas the human enzyme was reported to bind two Zn(II)

* This work was supported by National Institutes of Health Grants GM40075 (to M. W. C.), AI056231, and EB001980 (to B. B.) and National Science Foundation Grant MCB-0041105 (to C. A. M.). The costs of publication of this article were defrayed in part by the payment of page charges. This article must therefore be hereby marked "*advertisement*" in accordance with 18 U.S.C. Section 1734 solely to indicate this fact.

[1] To whom correspondence should be addressed: Dept. of Chemistry and Biochemistry, Miami University, 160 Hughes Hall, Oxford, OH 45056. Tel.: 513-529-7274; Fax: 513-529-5715; E-mail: crowdemw@muohio.edu.

[2] The abbreviations used are: GLX1, glyoxalase I; GLX2, glyoxalase II; FPLC, fast performance liquid chromatography; MG, methylglyoxal; MOPS, 3-(*N*-morpholino)propanesulfonic acid; PIXE, particle-induced X-ray emission; SLG, *S*-D-lactoylglutathione.

ions (42). The crystal structure of human cytoplasmic GLX2 showed that one metal-binding site consisted of three conserved histidine residues, a bridging aspartic acid, and a bridging water/hydroxide. The second metal-binding site had 2 histidines, 1 bridging Asp, 1 terminally bound Asp, 1 bridging water/hydroxide, and 1 terminally bound water (42). These crystallographic data have shown that the structures of the metal-binding and active sites of GLX2 are similar to those of metallo-β-lactamase L1 from *Stenotrophomonas maltophilia* (43). It has been suggested recently that subtle differences in the metal-binding ligands of β-lactamase fold-containing proteins may be responsible for differences in metal binding properties between the different enzymes (44). This theory is supported by mutational studies on *Arabidopsis* GLX2-2, which have shown that mutations both inside and outside the metal-binding ligands can affect the relative amount and identity of metal bound by the enzyme (39). Therefore, metallo-β-lactamase fold-containing enzymes can bind several different metals and catalyze a number of different reactions.

The presence of mitochondrial isoforms of GLX2 is intriguing because the GLX1 and its product SLG have only been observed in the cytosol (1). Yet mitochondrial GLX2 from several sources appears to utilize SLG as its preferred substrate (24, 26, 28). Furthermore, overall sequence identity between the cytoplasmic and mitochondrial enzymes is typically limited to 30–40%. Thus, the physiological substrate(s) and the role(s) of mitochondrial GLX2 are not clear, and further research is required in order to obtain more detailed information on the mitochondrial enzymes.

In an effort to better understand the specific roles of the different GLX2 isozymes as well as to correlate structural and functional features of this important class of enzymes, we have begun a characterization of the GLX2 isozymes in *Arabidopsis thaliana*. Five genes have been identified to encode putative GLX2 isozymes in *A. thaliana* (23). In addition to GLX2-2, three GLX2 isozymes are localized in mitochondria (GLX2-1, GLX2-4, and GLX2-5). The fifth GLX2-like gene, *glx2-3*, encodes a protein that lacks many of the conserved substrate-binding residues and may not in fact encode a functional GLX2 enzyme.[3] To date, detailed structural and kinetic studies have only been conducted on the cytoplasmic isozyme of GLX2 (39–41). A mitochondrial GLX2 isozyme has not been studied in detail from any organism. Therefore, we have overexpressed, purified, and characterized the mitochondrial GLX2-5 isozyme from *Arabidopsis* using metal analysis, EPR and ^{1}H NMR spectroscopies, and x-ray crystallography.

Biochemical studies indicate that GLX2-5 is a FeZn protein that has a preference for SLG as its substrate. Multiple metal centers, including an anti-ferromagnetically coupled Fe(III)Fe(II) center, were identified by EPR spectra, but EPR and the crystal structure analysis showed that the predominant form of the enzyme contains an Fe(III)Zn(II) center.

These results represent the first detailed structural characterization of a mitochondrial GLX2 enzyme from any source. They demonstrate for the first time that β-lactamase fold-containing proteins can accommodate mixed metal centers and provide new insights into structure-function features associated with GLX2 enzymes in particular and β-lactamase fold-containing enzymes in general.

EXPERIMENTAL PROCEDURES

General—PCR reagents, Deep Vent DNA polymerase, restriction enzymes (NdeI and XhoI), and *S*-D-lactoylglutathione were purchased from Sigma and New England Biolabs (Beverly, MA). Primers were synthesized by Integrated DNA Technologies (Coralville, IA). All chromatographic steps were carried out on a fast protein liquid chromatography (FPLC; Amersham Biosciences) system operating at 4 °C. Columns and resins for FPLC were purchased from Amersham Biosciences. All protein and DNA quantitations were performed on an Agilent 8453 UV-visible spectrophotometer.

```
                10        20        30        40        50
AtGLX2-5: MQIELVPCLKDNYAYILHDEDTGTVGVVDPSEAEPIIDSLKRSGRNLTYI
          M++E++P L DNY Y++ D++T    +VDP + + ++D+ ++ G  LT +
HuGLX2-2: MKVEVLPALTDNYMYLVIDDETKEAAIVDPVQPQKVVDAARKHGVKLTTV

               60        70        80        90        100
AtGLX2-5: LNTHHHYDHTGGNLEL-KDRYGAKVIGSAMDKDRIPGIDMALKDGDKWMF
          L THHH+DH GGN +L K   G KV G     DRI  +   +
HuGLX2-2: LTTHHHWDHAGGNEKLVKLESGLKVYGG---DDRIGALTHKITHLSTLQV

              110       120       130       140
AtGLX2-5: AGHEVHVMDTPGHTKGHISLYF--PGSR---AIFTGDTMFSLSCGKLFEG
             V  + TP HT GHI  +   PG     A+FTGDT+F   CGK +EG
HuGLX2-2: GSLNVKCLATPCHTSGHICYFVSKPGGSEPPAVFTGDTLFVAGCGKFYEG

          150       160       170       180       190
AtGLX2-5: TPKQML-ASLQKITSLPDDTSIYCGHEYTLSNSKFALSLEPNNEVLQSYA
          T  +M  A L+ +  LP DT +YCGHEYT++N KFA  +EP N  ++
HuGLX2-2: TADEMCKALLEVLGRLPPDTRVYCGHEYTINNLKFARHVEPGNAAIREKL

          200       210       220       230       240
AtGLX2-5: AHVAELRSKKLPTIPTTVKMEKACNPFLRSSNTDIRRALRIPEAADEAEA
          A   E  S   PT+P+T+  E   NPF+R     +++        D
HuGLX2-2: AWAKEKYSIGEPTVPSTLAEEFTYNPFMRVREKTVQQH---AGETDPVTT

          250
AtGLX2-5: LGIIRKAKDDF
          +  +R+ KD F
HuGLX2-2: MRAVRREKDQF
```

FIGURE 1. **Sequence alignment of GLX2-5 from *A. thaliana* and GLX2 from human.** The numbering is based on the GLX2-5 sequence.

Overexpression and Purification of Arabidopsis GLX2-5—PCR was conducted on a GLX2-5 cDNA (39), with the primers CTCCCATATGCAAATTGAACTGGTGCCTT and CGAGGATCCTCGGTCGACGCTTTTTTTTTTTTTTTTT, which generated (NdeI and XhoI) sites at the 5′ and 3′ ends of the fragment, respectively. For expression in *Escherichia coli*, the leader sequence was removed by placing the N-terminal methionine at amino acid 71 of the predicted protein sequence. This construct yielded a protein with the same N terminus as the cytoplasmic form of the enzyme (Fig. 1). The 975-bp GLX2-5 PCR fragment was cloned into pT7-7 by using NdeI and XhoI. The resulting plasmid, GLX2-5/pT7-7, was transformed into DH10B *E. coli* cells, and the construct was verified by DNA sequencing.

The GLX2-5/pT7-7 plasmid was transformed into *E. coli* BL21 (DE3)-Rosetta cells and used for overexpression and protein purification as described previously (31). Protein production was induced by making the culture 0.2 mM in isopropyl thio-β-D-galactoside, and the culture was made 250 μM in $Fe(NH_4)_2(SO_4)_2$ and $Zn(SO_4)_2$. After induction at 15 °C for 24 h, the cells were harvested, washed three times with cold, sterile double distilled H_2O to remove salts, and the cell pellets were stored at −80 °C until further use.

The cell pellet was resuspended in 30 ml of 10 mM MOPS, pH 7.2, containing 0.1 mM phenylmethylsulfonyl fluoride. The cells were lysed by passage twice through a French press at 16,000 p.s.i., and the cell debris was removed by centrifugation at 12,500 rpm for 45 min. The cleared supernatant was purified using fast protein liquid chromatography (FPLC) with a Q-Sepharose column as described previously (31). Enzyme concentrations were determined by measuring the absorbance at 280 nm and using a molar extinction coefficient of 37,800 $M^{-1}cm^{-1}$. The molar extinction coefficient was determined by particle-induced x-ray emission (PIXE) experiments (46), which were conducted by Dr. W. Meyer-Klaucke at EMBL Outstation, Hamburg, Germany, as described previously (38).

[3] S. Rhee and C. A. Makaroff, unpublished results.

Metal Analyses—Metal analyses were performed on a Varian-Liberty 150 inductively coupled plasma spectrometer with atomic emission spectroscopy detection as described elsewhere (31). The concentration of GLX2-5 was 10 μM in 10 mM MOPS buffer, pH 7.2. A calibration curve with five standards and a correlation coefficient of greater than 0.998 was generated using Zn, Mn, Fe, and Cu reference solutions. The following emission wavelengths were chosen to ensure the lowest detection limits possible: Zn, 213.856 nm; Mn, 257.610 nm; Fe, 259.940 nm; and Cu, 324.754 nm. Metal concentrations were obtained and averaged from at least three enzyme preparations.

Steady-state Kinetic Studies—A series of thiol esters of glutathione were used for the preliminary investigation of substrate preferences of GLX2-5. The substrates used were *S*-D-lactoylglutathione (SLG, ϵ_{240} 3,100 M^{-1} cm^{-1}), *S*-mandeloylglutathione (ϵ_{263} 4,200 M^{-1} cm^{-1}), *S*-acetylglutathione (ϵ_{240} 2,980 M^{-1} cm^{-1}), *S*-acetoacetylglutathione (ϵ_{240} 3,400 M^{-1} cm^{-1}), *S*-formylglutathione (ϵ_{240} 3,300 M^{-1} cm^{-1}), *S*-glycolylglutathione ($\epsilon\epsilon_{240}$ 3,260 M^{-1} cm^{-1}), and *S*-lactonylglutathione ($\epsilon\epsilon_{240}$ 3,310 M^{-1} cm^{-1}). With the exception of SLG, all substrates were synthesized as described elsewhere (47). Thiol ester hydrolysis was monitored at 240 nm (except *S*-mandeloylglutathione, 263 nm) over 30 s at 25 °C. The concentrations of substrate and enzyme used were 200 and 10 μM, respectively.

The steady-state kinetic parameters of the GLX2-5-catalyzed hydrolysis of *S*-D-lactoylglutathione were determined at 25 °C in 10 mM MOPS, pH 7.2, using an Agilent 5483 Diode Array UV-visible spectrophotometer. The rate of hydrolysis was monitored by measuring the absorbance at 240 nm from 30 to 600 μM *S*-D-lactoylglutathione over a 30-s reaction period, and the data were analyzed as reported previously (31).

EPR Spectroscopy—EPR spectra were recorded on a Bruker ESP-300E spectrometer equipped with an Oxford Instruments ESR-900 helium flow cryostat operating at 4.7 K with 2 milliwatts of microwave power at 9.48 GHz and employing 10-G field modulation at 100 kHz. EPR samples contained 345 μM GLX2-5 in 10 mM MOPS, pH 7.2.

^{1}H NMR Spectroscopy—NMR samples of GLX2-5 contained ~10% D_2O for locking, and the concentration was 1.8 mM. The samples in D_2O were made by performing three or more dilution/concentration cycles in a Centricon-10 to a final concentration of 1.6–1.8 mM. The samples were then loaded into Wilmad 5-mm tubes for NMR. NMR spectra were collected on a Bruker Avance 500 spectrometer operating at 500.13 MHz, 298 K, and a magnetic field of 11.7 tesla, recycle delay (*AQ*), 41 ms; sweep width, 400 ppm. Protein chemical shifts were calibrated by assigning the H_2O signal the value of 4.70 ppm. A modified presaturation pulse sequence (zgpr) was used to suppress the proton signals originating from water molecules.

X-ray Crystallography—GLX2-5 was prepared and purified as described under "Overexpression and Purification of *Arabidopsis* GLX2-5." Enzyme purity was ascertained by SDS-PAGE to be >95%, and the concentration was 12 mg/ml (0.4 mM). The sample (2 ml) was drop-frozen in liquid nitrogen and shipped on dry ice to the Center for Eukaryotic Structural Genomics, University of Wisconsin, Madison. The coordinates have been deposited in the Protein Data Bank (accession number 1XM8).

Molecular Weight Determination—Approximately 5 mg of GLX2-5 was mixed with 7 mg of ovalbumin, 10 mg of ribonuclease A, and 1 mg of blue dextran and subjected to chromatography through a Sephadex S200 column in 10 mM MOPS, pH 7.2, containing 0.15 M NaCl. The flow rate was 1 ml/min, and 2.0-ml fractions were collected. Samples containing protein were identified by monitoring A_{280} and by SDS-PAGE. A sample of GLX2-5 was run as a control.

RESULTS

Overexpression, Purification, and Characterization of GLX2-5—Sequence comparisons of different GLX2 isozymes in *Arabidopsis* showed that GLX2-5 has a relatively long N-terminal extension that is predicted to target it for localization in the mitochondrion (23). To overexpress GLX2-5 in *E. coli*, this N-terminal leader was removed during subcloning to generate an N terminus of the protein, MQIELVP, which is similar to that in cytosolic GLX2-2 (23). This modified gene was inserted into pT7-7 to generate the overexpression plasmid *glx2-5*/pT7-7. This construct was transformed into *E. coli* BL21(DE3) Rosetta cells, and small scale growth cultures were used to optimize overexpression conditions for GLX2-5.

During purification using Q-Sepharose chromatography, GLX2-5 eluted from the column at ~125 mM NaCl, pH 7.2. SDS-PAGE showed that the purified enzyme was >95% pure (data not shown). The eluted protein was initially light blue in color; however, the coloration faded within 15–30 min. The procedure described under "Experimental Procedures" resulted in the highest yield of soluble, overexpressed GLX2-5, and resulted in ~50 mg of purified GLX2-5 from a 1-liter of culture.

Metal analyses on GLX2-5, overexpressed in the presence of 250 μM $Fe(NH_4)_2(SO_4)_2$ and $Zn(SO_4)_2$ in the culture medium, resulted in a purified recombinant enzyme that bound 1.04 ± 0.15 eq of iron, 1.31 ± 0.05 eq of Zn(II), 0.016 ± 0.02 eq of manganese, and <0.001 eq of copper. When GLX2-5 was overexpressed in media with no added iron or zinc, the resulting enzyme bound 0.61 ± 0.07 eq of iron, 0.58 ± 0.15 eqof Zn(II), and no detectable amounts of manganese or copper. Even though this latter sample of GLX2-5 still bound approximately equal amounts of Fe and Zn, the total metal content of the enzyme was roughly only 1.0. Therefore, the overexpression and purification procedure described under "Experimental Procedures" was used to prepare GLX2-5 for all subsequent studies.

Most glyoxalase II enzymes showed a preference for *S*-D-lactoylglutathione as the substrate, but as described above, SLG has not yet been found in the mitochondrion. Therefore, seven related thioesters of glutathione were used to determine the substrate preference of GLX2-5. The substrates used were *S*-lactoylglutathione, *S*-mandeloylglutathione, *S*-acetylglutathione, *S*-acetoacetylglutathione, *S*-formylglutathione, *S*-glycolylglutathione, and *S*-lactonylglutathione. Initial rate assays on these substrates showed that SLG was the preferred substrate. It showed an initial rate of hydrolysis of 2.96×10^{-6} M s^{-1}. *S*-Acetoacetylglutathione (1.33×10^{-6} M s^{-1}) and *S*-glycolylglutathione (0.90×10^{-6} M s^{-1}) were hydrolyzed at about half the rate of SLG, whereas *S*-mandeloylglutathione (0.35×10^{-6} M s^{-1}), *S*-acetylglutathione (0.32×10^{-6} M s^{-1}), and *S*-lactonylglutathione (0.29×10^{-6} M s^{-1}) were hydrolyzed at rates about 10-fold lower than SLG. *S*-Formylglutathione was not utilized as a substrate by GLX2-5.

Steady-state kinetic studies were then conducted on recombinant GLX2-5 at 25 °C using SLG as the substrate. The enzyme exhibited a k_{cat} of 129 ± 10 s^{-1} and a K_m of 391 ± 48 μM. These values are on the order of those observed for *Arabidopsis* GLX2-2, suggesting that SLG is the preferred substrate for GLX2-5.

Spectroscopic Studies on GLX2-5—The EPR spectrum of GLX2-5 (Fig. 2) is complex containing four distinct components. The two main components of the spectrum are interpreted to result from a protein-bound, magnetically isolated Fe(III) ion and an anti-ferromagnetically spin-coupled Fe(II)-Fe(III) system, which are described in detail below. In addition, the spectrum contains several minor components. Two of the minor components are likely contaminating species; adventitiously bound Mn(II) gives rise to a six-line pattern centered at $g_{eff.} = 2.0$ and an isotropic signal at $g_{eff.} = 4.3$ indicative of the presence of mononuclear

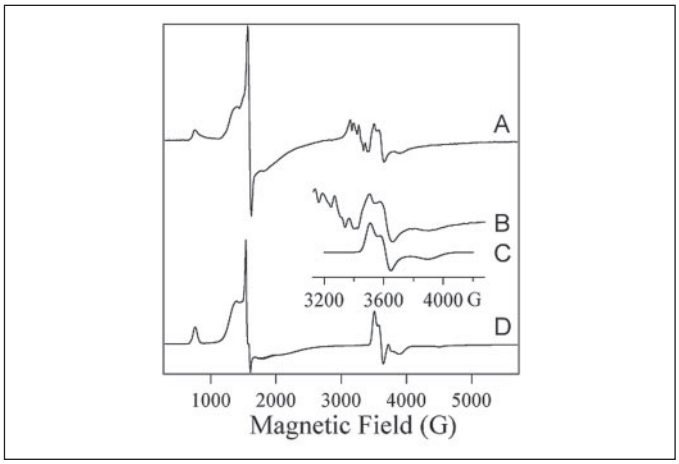

FIGURE 2. **EPR spectrum of GLX2-5.** *Trace A* shows the spectrum of GLX2-5 recorded at 4.7 K. The *inset* shows an expanded view of the $g \sim 1.9$ region of the spectrum (*trace B*) and a theoretical spectrum (*trace C*). The theoretical spectrum was generated using the spin Hamiltonian $H = \beta g_1.B.S_1 + S_1.D_1.S_1 + \beta g_2.B.S_2 + S_2.D_2.S_2 + J.S_1.S_2$, where $S_1 = 5/2$; $g_{1(iso)} = 2.0$; $D_1 = 3\ cm^{-1}$; $E_1 = 0$; $S_2 = 1$; $g_{2(x,y,z)} = 2.093$, 2.192, and 2.322; $D_2 = 10\ cm^{-1}$; $E = 0$; and $J = 50\ cm^{-1}$. This scheme represents a strongly anti-ferromagnetically coupled Fe(III)-Fe(II) center. *Trace D* shows a composite simulation of the experimental EPR spectrum. The simulation has two components, one of which is that shown as *trace C*, and another, the major component, corresponds to an isolated Fe(III) ion with $H = \beta g.B.S + S.D.S$, where $g_{(iso)} = 2.0$; $S = 5/2$; $D = 0.45\ cm^{-1}$; $E = 0.0855\ cm^{-1}$ ($E/D = 0.19$); $\Delta D = 0.20\ cm^{-1}$; and $\Delta E = 0.057\ cm^{-1}$. An additional component with an isotropic $g_{(eff)} = 4.3$ is present but was not included in the simulation.

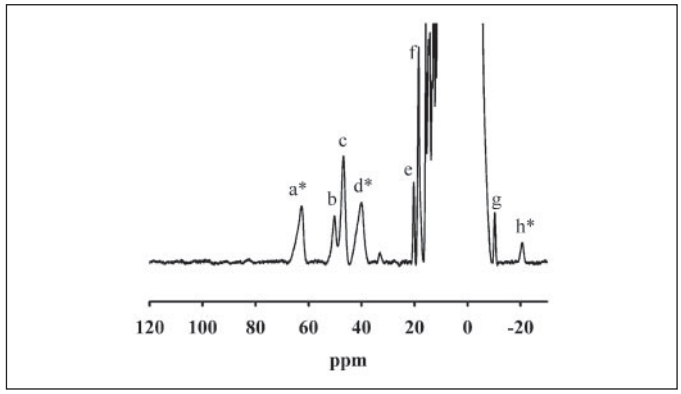

FIGURE 3. **NMR spectrum of 1. 6 mM GLX2-5.** NMR spectra were collected on a Bruker Avance 500 spectrometer operating at 500.13 MHz, 298 K, and a magnetic field of 11.7 tesla, recycle delay (*AQ*), 41 ms; sweep width, 400 ppm. Protein chemical shifts were calibrated by assigning the H_2O signal the value of 4.70 ppm. A modified presaturation pulse sequence (zgpr) was used to suppress the proton signals originating from water molecules. *, solvent-exchangeable peaks.

Fe(III). These two components are commonly seen in the EPR spectra of metalloenzymes and are present at low levels in the spectrum of GLX2-5. Integration of the spectra of $S > ½$ species is notoriously unreliable, especially when D is small and multiple Kramers' doublets are populated, some of which have resonances for which $g_{eff.}$ tends to zero. Nevertheless, in the present case the experimental spectrum, trace A, can be compared with a simulated spectrum, trace D, that does not contain these components. The six-line Mn(II) signal and the $g_{eff.} = 4.3$ isotropic signal are not major components of the spectrum of GLX2-5 and are likely irrelevant to the structure and function of the active site; therefore, they were not studied further.

The major species in the EPR spectrum of GLX2-5 can be confidently assigned to an unusual, protein-bound, magnetically isolated Fe(III) ion on the basis of computer simulation. The experimental spectrum (Fig. 2, *trace A*) shows a peak at 750 G ($g_{eff.} = 9.01$), a broad peak at 1410 G, a derivative at 1595 G ($g_{eff.} = 4.25$ G), and a shoulder at 1815 G with broad underlying absorption. Considering the sensitivities of the intensities, resonance positions, and line shapes of these features to not only the zero-field splitting parameters themselves but, in particular, to the effects of strains in g, D, and E, the theoretical spectrum shown as Fig. 1, *trace D*, reproduces the features of the experimental spectrum remarkably well. The detailed parameters used for the simulation are given in the legend to Fig. 1, but the salient points are as follows: (i) an isotropic $g = 2.0$; (ii) a moderately rhombic E/D; (iii) an unusually low value for D, barely larger than the microwave quantum; and (iv) significant strains in the zero-field splitting parameters. The simulations were extremely sensitive to D, E/D, ΔD, and ΔE; the simulation rapidly becomes unrecognizable as being related to the experimental spectrum upon changing these values, and we estimate maximum errors of ±15% for each of these parameters. The main deficiencies of the simulation are the imperfect reproduction of the sharp spike at $g_{eff.} \sim 4.2$ and the underestimation of the intensity of the broad absorption from 1600 to 2200 G. Both of these are likely the result of the overlapping isotropic $g_{eff.} = 4.3$ signal due to adventitious Fe(III), although it is possible that the strains in the zero-field splitting parameters have a more complex distribution than the simple one used in the present work. An additional minor difference between the simulation and experimental spectra is the presence of sharp but very weak features at ~3750 and ~4500 G in the simulation that are not observed experimentally; either strains in g or relaxation effects may be responsible for the absence of these features in the experimental spectrum.

The EPR spectrum of GLX2-5 contained, in addition to the protein-bound Fe(III) that constituted the major species, a rhombic signal with apparent $S = ½$ and $g_{eff.}$ values of 1.93, 1.87, and 1.73 (Fig. 2, *trace B*). As we are unaware of any mononuclear $S = ½$ ions that were likely to be present in our preparation that would give rise to these parameters, we were prompted to seek an alternative assignment for this signal. The signal was well simulated, assuming a strongly anti-ferromagnetically spin-coupled Fe(II)-Fe(III) system and assuming an isotropic $g_{Fe(III)} = 2.0$, a rhombic $g_{Fe(II)}$ with $g > 2.0$, and $J \gg h\nu$. It should be pointed out that there is no unique parameter set for generating this spectrum (or others very similar to it), and the detailed parameters used to obtain Fig. 2, *trace D*, are given in the figure legend mainly for reference. However, they do also serve to illustrate that the otherwise uninterpretable signal at $g_{eff.} = 1.93$, 1.87, and 1.73 can be interpreted in terms of an Fe(II)-Fe(III) mixed valence center using reasonable values for g, individual zero-field splittings, and exchange coupling. Assuming that the signal is indeed due to a di-iron center, and with caveats regarding the quantification of the major $S = 5/2$ signal in mind, we estimated that the $g_{eff.} = 1.93$, 1.87, 1.73 signal accounts for up to a maximum of 20% of the total protein-bound iron.

In order to probe further the active site structure of GLX2-5, a ^1H NMR spectrum of GLX2-5 was obtained (Fig. 3). There were at least eight paramagnetically shifted resonances in-between 110 and −30 ppm. Previous studies have shown that the T_{1e} of Fe(III) when part of a Fe(III)Zn(II) center is too slow to observe paramagnetically shifted ^1H resonances (48, 49). Therefore, the peaks observed in Fig. 3 must be due to ligands bound to a Fe(III)Fe(II) center in the sample., *Peaks a, c, d,* and *f* of Fig. 3 integrate to two protons, whereas *peaks b, g,* and *h* integrate to nearly 1 proton each. *Peaks a* and *d* of Fig. 3 are solvent-exchangeable, and based on their resonance positions and line widths, these peaks can be assigned to N-H protons on Fe(III)- and Fe(II)-bound histidines, respectively (48, 50, 51). This result suggests that there are at least four histidines bound to the Fe(III)Fe(II) center in this sample. If GLX2-5 is similar to human GLX2-2 then there should be five histidines bound to the metal center. It is possible that a fifth solvent-exchangeable NH resonance is not observed due to fast exchange with bulk solvent (49,

52). The solvent-exchangeable, upfield shifted peak h is very unusual because very few metal-binding amino acid ligands are solvent-exchangeable, and none are known to yield upfield shifted peaks. An upfield shift is suggestive of a π, rather than σ, delocalization mechanism (50). A similarly shifted, solvent-exchangeable peak was observed in Fe(III)Fe(II)-containing uteroferrin; however, the assignment of this peak has not been made (50). It has been suggested that this peak arises from a backbone NH in close proximity to the metal center (53). Although unambiguous assignments of the remaining peaks are not possible, it is likely that peaks b and c are due to either meta protons (−CH) on Fe(II)-bound histidines or to β-CH_2 protons on metal-bound histidines (49, 50). Ortho protons on metal-bound histidines are usually too broad to detect (50). Peaks f and g are probably due to β-CH_2 protons on bound Asp/Glu ligands (49, 50). Therefore, the NMR spectrum of GLX2-5 confirmed the presence of an Fe(III)Fe(II) center in the enzyme.

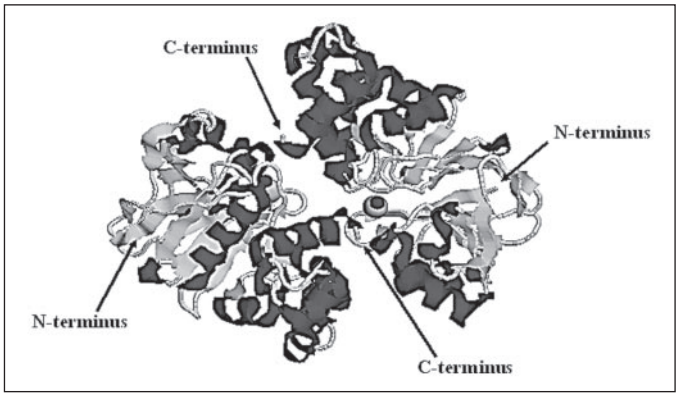

FIGURE 4. **Ribbon structure of GLX2-5 from *A. thaliana*.** The coordinates have been deposited in the Protein Data Bank (accession number 1XM8). Figure was rendered using Raswin Molecular Graphics, Windows version 2.7.2.1.1.

Crystallographic Studies on GLX2-5—Alignment of GLX2-5 with human GLX2 (Fig. 1) indicated that the proteins share modest sequence identity (37% identical). The largest blocks of identical residues are present around residues identified as metal-binding ligands in the human enzyme. Other regions (amino acids 69–132 and 187–257) demonstrated less sequence conservation. Furthermore, if GLX2-5 contains a Fe(III)Zn(II) structure as we predict, then the geometries of the metal centers of the two enzymes should differ. Therefore, the x-ray crystal structure of GLX2-5 at pH 4.5 was solved to 1.74 Å resolution and is shown in Fig. 4 (TABLES ONE and TWO). The enzyme crystallized as a dimer with monomers of 254 amino acids, and each monomer has an $\alpha\beta\beta\alpha$ motif, which is found in all enzymes containing a metallo-β-lactamase fold (44). The interface between the two monomers contains Lys-10, His-56, Tyr-57, Lys-140, Phe-142, Glu-143, Lys-177, Lys-203, Asp-253, and Phe-254 from both subunits. The dimer is held together by a number of electrostatic interactions such as Lys-10 forming contacts with Asp-11 and Glu-170, Asp-253 forming a contact with His-56, and Phe-254 hydrogen bonding to Tyr-57. One molecule of acetate was found in each subunit and was located near (distances <3.0 Å) Arg-248, Lys-251, Lys-140, and Ser-137. One molecule of PEG was found in subunit A and was shown to be positioned near Lys-202. The C terminus of each monomer lies in the dimer interface, which is solvent-accessible, whereas the N termini are solvent-exposable.

Each monomer binds two heavy atoms, and the metal ions are bound near the surfaces of the monomers in-between the β-sheets of the $\alpha\beta\beta\alpha$ motif. Because EPR studies predicted that a Fe(III)Zn(II) center is predominant in recombinant GLX2-5, this center is shown in Figs. 4 and 5. However, we cannot completely rule out the possibility of a dinuclear Fe or Zn center. The metal centers face one another with the metal ion in

TABLE ONE

Comparisons of the active sites of human GLX2-2 and A. thaliana GLX2-5

Structures for human GLX2-2 (Protein Data Bank number 1QH3) and *A. thaliana* GLX2-5 (Protein Data Bank number 1XM8) were analyzed with Raswin version 2.7.2.1.

Metal[a]	Enzyme	Residue	Atom	Distance	Bond angle (°)[b]	Second sphere ligands
				Å		
M1	GLX2-5	His-54	N-ϵ2	2.1	119	Thr-53
	GLX2-2	His-54	N-ϵ2	2.3	104	
M1	GLX2-5	His-56	N-δ1	2.1	104	
	GLX2-2	His-56	N-δ1	2.3	95	Glu-146 via water
M1	GLX2-5	His-112	N-ϵ2	2.1	129	Lys-140 carbonyl
	GLX2-2	His-110	N-ϵ2	2.3	161	
M1	GLX2-5	Bridging H_2O/OH^-		2.0		
	GLX2-2			2.1		
M1	GLX2-5	None				
	GLX2-2	Asp-134	O-δ2	2.2	78	Asp-134 carbonyl
M2	GLX2-5	Asp-58	O-δ2	2.0	90	
	GLX2-2	Asp-58	O-δ2	2.3	87	
M2	GLX2-5	His-59	N-ϵ2	1.9	107	Asp-29
	GLX2-2	His-59	N-ϵ2	2.2	101	
M2	GLX2-5	Asp-131	O-δ2	2.0	81	
	GLX2-2	Asp-134	O-δ2	2.2	78	
M2	GLX2-5	His-169	N-ϵ2	1.9	141	Asp-11
	GLX2-2	His-173	N-ϵ2	2.1	151	
M2	GLX2-5	Bridging H_2O/OH^-		2.1		
	GLX2-2			2.1		

[a] M1 is Zn(II) for both enzymes; M2 is Zn(II) for human GLX2-2 and Fe for *A. thaliana* GLX2-5.
[b] Bond angle is defined as the bridging H_2O/OH^- - metal-ligating atom of ligand.

TABLE TWO

Crystallographic and refinement statistics

Additional details about crystallographic and refinement statistics can be found on the Protein Data Bank, Research Collaboratory for Structural Bioinformatics website (Protein Data Bank number 1XM8).

Protein Data Bank number	1XM8
Space group	P1 21 1
Resolution range (Å)	33.71–1.74
Unique reflections	51,949
R_{merge} (%)[a]	7.9 (54.5)
$\langle I/\sigma(I)\rangle$ (%)[a]	21.2 (4.3)
Completeness (%)[a]	95.4 (97.4)
R/R_{free} (%)	17.9 / 28.4
Root mean square deviation bond length (Å)	0.020
Root mean square deviation bond angle (°)	1.7
No. water molecules	547
Method to solve structure	SAD[b]

[a] Values for the highest resolution shell are in parentheses.
[b] SAD is single wavelength anomalous diffraction.

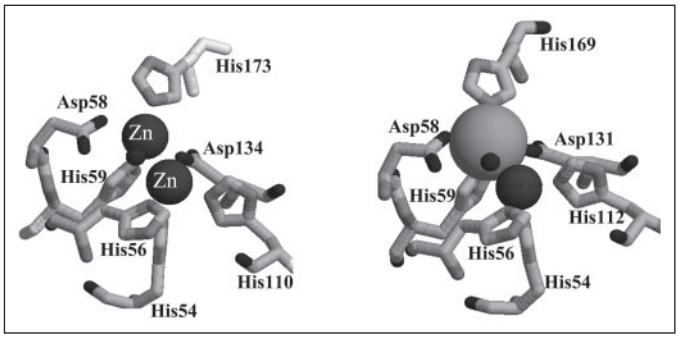

FIGURE 5. **Active sites of (*left*) GLX2-2 from human and (*right*) GLX2-5 from *A. thaliana*.** Figure was rendered using Raswin Molecular Graphics, Windows version 2.7.2.1.1.

site 1 of each subunit being 17.8 Å apart (Fig. 4). The metal ions in each subunit are separated by 3.3 (4) Å (Fig. 5). The metal ion in site 1 is coordinated tetrahedrally by His-54, His-56, His-112, and a bridging water/hydroxide (TABLE ONE). The metal ion in site 2 is coordinated in a trigonal bipyramid geometry by Asp-58, His-59, Asp-131, His-169, and a bridging water/hydroxide, with Asp-131 and Asp-58 in the apical positions of the trigonal bipyramid. One oxygen (O-δ1) of Asp-58 appears to be in position (2.78 Å from bridging hydroxide oxygen) to form a hydrogen bond to the bridging water/hydroxide. A similar role was predicted for Asp-120 in metallo-β-lactamase L1 (2.83 Å from O-δ1 to hydroxide oxygen) (43).

The crystal structure of human GLX2 complexed with glutathione and *S*-hydroxybromophenylcarbamoyl glutathione showed that Arg-249, Lys-252, Lys-143, Tyr-175, and Tyr-145 are within 13 Å of the metal ion in site 1 and interact with glutathione and *S*-hydroxybromophenylcarbamoyl glutathione. Alignment of the amino acid sequences of human GLX2 and GLX2-5 (Fig. 1) shows that all of the glutathione and inhibitor-binding residues of human GLX2 are conserved in GLX2-5 except Tyr-145, which is replaced by a Phe in GLX2-5. Phe-142, Tyr-171, Arg-248, Lys-140, and Lys-251 are all within 13 Å of the metal ion in site 1 of GLX2-5. Therefore, we predicted that these ligands are involved in substrate binding.

One common structural feature of enzymes that have a metallo-β-lactamase fold is an extensive H-bonding network around the metal-binding ligands (TABLE ONE). In particular, the ligands that coordinate the metal ion in site 2 typically form hydrogen bonds to two Asp residues. In GLX2-5, His-169 (N-δ1) forms an H-bond with O-δ1 of Asp-11

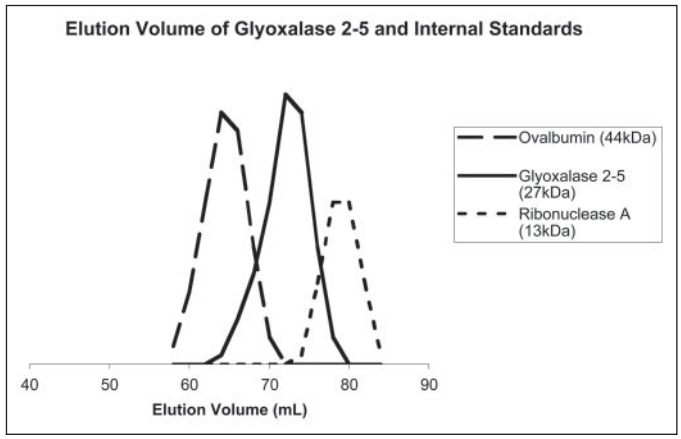

FIGURE 6. **Elution profile from gel filtration column.** Approximately 5 mg of GLX2-5, 7 mg of ovalbumin, 10 mg of ribonuclease A, and 1 mg of blue dextran were separated on a Sephadex S200 column. Samples containing protein were identified by monitoring A_{280} and by SDS-PAGE.

(2.86 Å), and Asp-11 (O-δ2) forms a hydrogen bond with the side chain of Lys-10. The O-δ2 oxygen of Asp-11 is also positioned to hydrogen-bond to a solvent molecule, which H-bonds to a second solvent molecule that hydrogen-bonds to Asp-11 (O-δ2) in molecule B of the structure. The N-δ1 nitrogen of His-59 forms a hydrogen bond to the O-δ2 of Asp-29 (2.819 Å), whereas the O-δ1 oxygen of Asp-29 forms a hydrogen bond to the backbone amine of Thr-53. The metal-binding ligands in site 2 also form hydrogen bonds with amino acids near the active site: N-δ1 of His-54 hydrogen bonds to the O-γ1 of Thr-53, and the carbonyl oxygen of Lys1–40 (which corresponds to Lys-143 in human GLX2) forms a hydrogen bond with the N-δ1 of His-112. Therefore, a similar hydrogen bonding network is conserved in GLX2-5.

GLX2-5 Exists as a Monomer in Solution—In contrast to the situation in the crystal structure, GLX2-5 was found to exist as a monomer when a sample of recombinant protein was subjected to gel filtration chromatography (Fig. 6). GLX2-5 was found to elute between ovalbumin (44 kDa) and ribonuclease A (13 kDa) during gel filtration chromatography. The molecular mass of the recombinant GLX2-5 monomer is 28.2 kDa, whereas a dimer would be expected to run as a 56-kDa protein. It is possible that weak interactions between the GLX2-5 monomers result in some dimerization of the enzyme in the cell that are disrupted by the ionic strength of the buffer during gel filtration. However, it is more likely that the dimers observed in the crystal structure of both GLX2-5 and human GLX2 are likely the result of the conditions used for crystallization.

DISCUSSION

Mitochondrial GLX2-5 from *A. thaliana* was successfully overexpressed and purified with single step chromatography. The resulting protein was shown to bind significant amounts of both Fe and Zn(II), but unlike *Arabidopsis* GLX2-2 (40, 41), very little Mn was bound to the enzyme. The complex EPR spectra of GLX2-5 are very reminiscent of those of *Arabidopsis* GLX2-2 (40, 41), which contain overlapping signals that have been assigned to Fe(III)Zn(II), anti-ferromagnetically coupled Fe(III)Fe(II), and ferromagnetically coupled Mn(II)Mn(II) centers. However, there are no signals that could be assigned to a ferromagnetically coupled Mn(II)Mn(II) center in the spectrum of GLX2-5, and the relatively weak, multiline signal at $g \sim 2$ is probably due to adventitiously bound, mononuclear Mn(II). The EPR spectrum of GLX2-5 does suggest the presence of a magnetically uncoupled Fe(III) center that, given the metal analyses and precedents in the literature (45, 54, 55), can be assigned to a Fe(III)Zn(II) center. This center is the predominant one

in GLX2-5 accounting for nearly 70% of the EPR-active Fe(III) in the spectrum. There is also a significant amount of an anti-ferromagnetically coupled Fe(III)Fe(II) center, which accounts for nearly 30% of the Fe in the sample. Because there are roughly equal amounts of Fe and Zn in GLX2-5, there must also be a significant amount of dinuclear Zn(II)-containing enzyme in this sample. Therefore, like recombinant GLX2-2 (40, 41), recombinant mitochondrial GLX2-5 contains a mixture of metal centers.

The ^{1}H NMR spectrum of GLX2-5 arises from protons in close proximity to the Fe(III)Fe(II) center in the sample. The crystal structure of GLX2-5 (Fig. 5) shows that there are five bound histidines to the metal center; however, the NMR spectra only revealed four solvent-exchangeable NH resonances. The crystal structure (Fig. 5) shows that the NH group on His-56 is pointed directly into the media, and this positioning provides an excellent explanation of why the fifth solvent-exchangeable NH resonance is not observed. His-56 is also the only histidine that is bound via the δN; therefore, there would only be one *meta*-CH proton expected in the NMR spectrum. Previous model studies by Que and co-workers (50) revealed that meta protons on imidazoles/histidines bound to Fe(III) exhibit resonance lines from 70 to 90 ppm, whereas those bound to Fe(II) exhibit resonances from 30 to 60 ppm. Because there are no resonances in the 70–90-ppm region (Fig. 3) that could be assigned to a meta proton, this result indicates that His-56 is coordinated to an Fe(II). Because it is most likely that Zn(II) will replace Fe(II) in the Fe(III)Zn(II) analog of GLX2-5, this result suggests that the metal bound in the site containing His-56 in Fig. 5 is Zn(II).

To probe further the structure of GLX2-5, the enzyme was sent to the Center for Eukaryotic Structural Genomics for crystal structure determination. Even though our spectroscopic results indicate that the GLX2-5 sample is heterogeneous in terms of metal centers, this sample yielded suitable crystals for structure determination. Although similar in many ways, the crystal structures of human GLX2 and GLX2-5 show some significant structural differences between the two enzymes. Both enzymes crystallized as dimers; however, the dimer interface in human GLX2 is made up entirely of α-helices in the C termini of the monomers. The metal centers in human GLX2 face each other but are separated by >36 Å. Conversely, the dimer interface in GLX2-5 is extensive with multiple interactions between amino acids in each monomer and a Zn(II)-Zn(II) distance of 18 Å (Fig. 4).

Perhaps more interesting are our results concerning the metal centers in the two enzymes, which also show several differences. The crystal structure of human GLX2 showed two Zn(II) ions separated by 3.4–3.5 Å, and each Zn(II) was coordinated by six ligands in an octahedral geometry (42). The metal ions in GLX2-5 are coordinated by the same amino acid ligands that coordinate the Zn(II) ions in human GLX2. However, there is no evidence for additional solvent molecules coordinated to the metal ions in GLX2-5, and the metal ions have trigonal bipyramidal and tetrahedral geometries. The Zn(II) ions in human GLX2 are bridged by a hydroxide and by O-δ2 of Asp-134 (42), whereas there is no evidence of a bridging Asp (Asp-131) in GLX2-5. Despite missing the bridging Asp, the M–M bond distance is 0.1 Å shorter in GLX2-5 than in the human enzyme (42). In addition, the metal-ligand distances are shorter in GLX2-5 than in human GLX2-2 (TABLE ONE). There are also large differences in the bond angles (bridging hydroxide/water-metal-atom in ligand) in the active sites of the two enzymes (TABLE ONE).

Despite the differences in metal ions and their geometry and in some first sphere ligands in human GLX2 and GLX2-5, the hydrogen bonding network around the metal centers is remarkably conserved. Asp-11 and Asp-29 form H-bonds to the metal-binding histidines in the Zn_2 site of human GLX2 (42), and these same residues form hydrogen bonds with metal-binding ligands of site 2 in GLX2-5. The different metal contents of the two enzymes cannot be directly attributed to different metal ligands, but may be related to different second sphere interactions. Two of the second sphere ligands in human GLX2 (Thr-53 and Lys-143 (Lys-140 in GLX2-5)) form interactions with His residues of site 1 in GLX2-5. However, two key second sphere ligand interactions observed in the structure of human GLX2 are missing in GLX2-5. Glu-146 (incorrectly labeled Asp-146 in Table 1 of Ref. 42) was shown to interact with His-56, via a water molecule, in the structure of human GLX2. There is no evidence of a water molecule in the structure of GLX2-5 between His-56 and Glu-143, and these two residues are 5.2 Å apart and probably do not interact. The structure of human GLX2 also suggested an interaction of the carbonyl of Asp-134 with the side chain of Asp134 (42); this interaction is not observed in GLX2-5. At this time it is not clear if these differences in second sphere influence the metal binding properties of the enzyme or if they result from the different geometries of the metal centers in GLX2-5.

Results presented in this study represent the first detailed structural characterization of a mitochondrial glyoxalase 2 isozyme from any source. Our results indicate that although the *Arabidopsis* GLX2 isozymes can utilize a number of different metal centers, it appears that a Fe(III)Zn(II) center is the predominant form of GLX2-5. Although further studies are required on other GLX2 and β-lactamase fold-containing enzymes to better understand factors that control metal specificity in these enzymes, our results suggest that subtle alterations in second sphere ligands may directly affect metal preference and geometry in GLX2 enzymes. Differences in second sphere ligands may explain why human GLX2 appears to have a preference for a dinuclear Zn site, whereas the majority of recombinant *Arabidopsis* GLX2-5 contains a Fe(III)Zn(II) site. What role, if any, differences in metal center preference and geometry play in the catalytic mechanism remains to be determined.

Acknowledgments—We thank Wolfram Meyer-Klaucke from the EMBL Outstation, Hamburg, Germany, for performing the PIXE experiments. We also thank Damodaran Krishnan for assistance in obtaining the NMR spectra and G. E. Wesenberg, D. W. Smith, G. N. Phillips, Jr., E. Bitto, C. A. Bingman, and S. T. M. Allard at the Center for Eukaryotic Structural Genomics, University of Wisconsin, for determining the crystal structure of GLX2-5. Funds to purchase the 500-MHz NMR were provided by the Hayes Investment Fund (Ohio Board of Regents).

REFERENCES

1. Thornalley, P. (1993) *Mol. Aspects Med.* **14,** 287–371
2. Davidson, G., Clugston, S. L., Honek, J. F., and Maroney, M. J. (2000) *Inorg. Chem.* **39,** 2962–2963
3. Thornalley, P. J. (1998) *Chem. Biol. Interact.* **111,** 137–151
4. Thornalley, P. (1995) *Crit. Rev. Oncol. Hematol.* **20,** 99–128
5. Papoulis, A., Al-Abed, Y., and Bucala, R. (1995) *Biochemistry* **34,** 648–655
6. Rahman, A., Shahabuddin, A., and Hadi, S. (1990) *J. Biochem. Toxicol.* **5,** 161–166
7. Lo, T., Westwood, M., McLellan, A., Selwood, T., and Thornalley, P. (1994) *J. Biol. Chem.* **269,** 32299–32305
8. Rulli, A., Carli, L., Romani, R., Baroni, T., Giovannini, E., Rosi, G., and Talesa, V. (2001) *Breast Cancer Res. Treat.* **66,** 67–72
9. Thornalley, P. J. (1993) *Biochem. Soc. Trans.* **21,** 531–534
10. Norton, S. J., Elia, A. C., Chyan, M. K., Gillis, G., Frenzel, C., and Principato, G. B. (1993) *Biochem. Soc. Trans.* **21,** 545–548
11. Allen, R. E., Lo, T. W. C., and Thornalley, P. J. (1993) *Biochem. Soc. Trans.* **21,** 535–539
12. Creighton, D. J., Zheng, Z.-B., Holewinski, R. J., Hamilton, D. S., and Eiseman, J. L. (2003) *Biochem. Soc. Trans.* **31,** 1378–1382
13. Thornalley, P. J., Strath, M., and Wilson, R. J. H. (1994) *Biochem. Pharmacol.* **47,** 418–420
14. McLellan, A. C., Thornalley, P. J., Benn, J., and Sonksen, P. H. (1994) *Clin. Sci.* (*Lond.*)

87, 21–29
15. Ratliff, D. M., Vander Jagt, D. J., Eaton, R. P., and Vander Jagt, D. L. (1996) *J. Clin. Endocrinol. Metab.* **81,** 488–492
16. Chen, F., Wollmer, M. A., Hoerndli, F., Munch, G., Kuhla, B., Rogaev, E. I., Tsolaki, M., Papassotiropoulos, A., and Gotz, J. (2004) *Proc. Natl. Acad. Sci. U. S. A.* **101,** 7687–7692
17. Creighton, D. J., and Hamilton, D. S. (2001) *Arch. Biochem. Biophys.* **387,** 1–10
18. Richter, U., and Krauss, M. (2001) *J. Am. Chem. Soc.* **123,** 6973–6982
19. Sharkey, E. M., O'Neill, H. B., Kavarana, M. J., Wang, H. B., Creighton, D. J., Sentz, D. L., and Eiseman, J. L. (2000) *Cancer Chemother. Pharmacol.* **46,** 156–166
20. Kavarana, M. J., Kovaleva, E. G., Creighton, D. J., Wollman, M. B., and Eiseman, J. L. (1999) *J. Med. Chem.* **42,** 221–228
21. Cordell, P. A., Futers, T. S., Grant, P. J., and Pease, R. J. (2004) *J. Biol. Chem.* **279,** 28653–28661
22. Bito, A., Haider, M., Hadler, I., and Breitenbach, M. (1997) *J. Biol. Chem.* **272,** 21509–21519
23. Maiti, M. K., Krishnasamy, S., Owen, H. A., and Makaroff, C. A. (1997) *Plant Mol. Biol.* **35,** 471–481
24. Talesa, V., Uotila, L., Koivusalo, M., Principato, G., Giovannini, E., and Rosi, G. (1989) *Biochim. Biophys. Acta* **993,** 7–11
25. Talesa, V., Uotila, L., Koivusalo, M., Principato, G., Giovannini, E., and Rosi, G. (1988) *Biochim. Biophys. Acta* **955,** 103–110
26. Bito, A., Haider, M., Briza, P., Strasser, P., and Breitenbach, M. (1999) *Protein Expression Purif.* **17,** 456–464
27. Norton, S. J., Talesa, V., Yuan, W. J., and Principato, G. B. (1990) *Biochem. Int.* **22,** 411–418
28. Talesa, V., Rosi, G., Contenti, S., Mangiabene, C., Lupattelli, M., Norton, S. J., Giovannini, E., and Principato, G. B. (1990) *Biochem. Int.* **22,** 1115–1120
29. Talesa, V., Principato, G. B., Norton, S. J., Contenti, S., Mangiabene, C., and Rosi, G. (1990) *Biochem. Int.* **20,** 53–58
30. Talesa, V., Rosi, G., Bistoni, F., Marconi, P., Norton, S. J., and Principato, G. B. (1990) *Biochem. Int.* **21,** 397–403
31. Crowder, M. W., Maiti, M. K., Banovic, L., and Makaroff, C. A. (1997) *FEBS Lett.* **418,** 351–354
32. Ridderstrom, M., and Mannervik, B. (1997) *Biochem. J.* **322,** 449–454
33. Ridderstrom, M., Saccucci, F., Hellman, U., Bergman, T., Principato, G., and Mannervik, B. (1996) *J. Biol. Chem.* **271,** 319–323
34. Irsch, T., and Krauth-Siegel, R. L. (2004) *J. Biol. Chem.* **279,** 22209–22217
35. Crowder, M. W., and Walsh, T. R. (1999) *Res. Signpost* **3,** 105–132
36. Cricco, J. A., and Vila, A. J. (1999) *Curr. Pharm. Des.* **5,** 915–927
37. Frazao, C., Silva, G., Gomes, C. M., Matias, P., Coelho, R., Sieker, L., Macedo, S., Liu, M. Y., Oliveira, S., Teixeira, M., Xavier, A. V., Rodrigues-Pousada, C., Carrondo, M. A., and Le Gall, J. (2000) *Nat. Struct. Biol.* **7,** 1041–1045
38. Vogel, A., Schilling, O., Niecke, M., Bettmer, J., and Meyer-Klaucke, W. (2002) *J. Biol. Chem.* **277,** 29078–29085
39. Zang, T. M., Hollman, D. A., Crawford, P. A., Crowder, M. W., and Makaroff, C. A. (2001) *J. Biol. Chem.* **276,** 4788–4795
40. Schilling, O., Wenzel, N., Naylor, M., Vogel, A., Crowder, M., Makaroff, C., and Meyer-Klaucke, W. (2003) *Biochemistry* **42,** 11777–11786
41. Wenzel, N. F., Carenbauer, A. L., Pfiester, M. P., Schilling, O., Meyer-Klaucke, W., Makaroff, C. A., and Crowder, M. W. (2004) *J. Biol. Inorg. Chem.* **9,** 429–438
42. Cameron, A. D., Ridderstrom, M., Olin, B., and Mannervik, B. (1999) *Structure* (*Lond.*) **7,** 1067–1078
43. Ullah, J. H., Walsh, T. R., Taylor, I. A., Emery, D. C., Verma, C. S., Gamblin, S. J., and Spencer, J. (1998) *J. Mol. Biol.* **284,** 125–136
44. Melino, S., Capo, C., Dragani, B., Aceto, A., and Petruzzelli, R. (1998) *Trends Biochem. Sci.* **23,** 381–382
45. Yu, L., Haddy, A., and Rusnak, F. (1995) *J. Am. Chem. Soc.* **117,** 10147–10148
46. Johansson, S. A. E., and Campbell, J. L. (1988) *PIXE: A Novel Technique for Elemental Analysis*, pp. 1–347, John Wiley & Sons, Inc., New York
47. Uotila, L. (1981) *Methods Enzymol.* **77,** 424–430
48. Borovik, A. S., Papaefthymiou, V., Taylor, L. F., Anderson, O. P., and Que, L. (1989) *J. Am. Chem. Soc.* **111,** 6183–6195
49. Battistuzzi, G., Dietrich, M., Locke, R., and Witzel, H. (1997) *Biochem. J.* **323,** 593–596
50. Lauffer, R. B., Antanaitis, B. C., Aisen, P., and Que, L. (1983) *J. Biol. Chem.* **258,** 14213–14218
51. Wang, Z., Ming, L. J., Que, L., Vincent, J. B., Crowder, M. W., and Averill, B. A. (1992) *Biochemistry* **31,** 5263–5268
52. Bertini, I., Turano, P., and Vila, A. J. (1993) *Chem. Rev.* **93,** 2833–2932
53. Scarrow, R. C., Pyrz, J. W., and Que, L. (1990) *J. Am. Chem. Soc.* **112,** 657–665
54. Beck, J. L., de Jersey, J., Zerner, B., Hendrich, M. P., and Debrunner, P. G. (1988) *J. Am. Chem. Soc.* **110,** 3317–3318
55. Merkx, M., and Averill, B. A. (1998) *Biochemistry* **37,** 11223–11231